Biophysical Chemistry 42 (1992) 29–48
Elsevier Science Publishers B.V., Amsterdam

BIOCHE 01613

Analysis of photoacoustic waveforms using the nonlinear least squares method

Jeanne Rudzki Small *, Louis J. Libertini and Enoch W. Small

Department of Chemistry and Biochemistry, Eastern Washington University, Cheney, WA 99004 (USA)

(Received 23 January 1991; accepted in revised form 29 May 1991)

Abstract

Pulsed-laser photoacoustics is a technique which measures photoinduced enthalpic and volumetric changes on the nano- and microsecond timescales. Analysis of photoacoustic data generally requires deconvolution for a sum of exponentials, a procedure which has been developed extensively in the field of time-resolved fluorescence decay. Initial efforts to adapt an iterative nonlinear least squares computer program, utilizing the Marquardt algorithm, from the fluorescence field to photoacoustics indicated that significant modifications were needed. The major problem arises from the wide range of transient decay times which must be addressed by the photoacoustic technique. We describe an alternative approach to numerical convolution with exponential decays, developed to overcome the problems. Instead of using an approximation method (Simpson's rule) for evaluating the convolution integral, we construct a continuous instrumental response function by quadratic fitting of the discrete data and evaluate the convolution integral directly, without approximations. The success and limitations of this quadratic-fit convolution program are then demonstrated using simulated data. Finally, the program is applied to the analysis of experimental data to compare the resolution capabilities of two commercially available transducers. The advantages of a broadband, heavily damped transducer are shown for a standard organic photochemical system, the quenching of the triplet state of benzophenone by 2,5-dimethyl-2,4-hexadiene.

Keywords: Pulsed-laser photoacoustics; Data analysis; Nonlinear least squares; Ultrasonic transducers

1. Introduction

The technique of pulsed-laser, time-resolved photoacoustics has become increasingly popular in the last decade and is used to address physical, chemical and biological processes occurring on fast timescales, principally ns and μs. Applications of pulsed-laser photoacoustics have been recently reviewed [1–6]. In addition to its use for calorimetry and kinetics, the technique can be used to study photoinduced transient volume changes in molecules, such as conformational changes in proteins [7–10]. As the applications become more diverse, it is clear that there is increasing need to obtain high-quality experimental data and to develop more advanced ways of analyzing these data.

Most pulsed-laser photoacoustic methods rely on a comparison of the photoacoustic waveform

* Please address correspondence to Dr. J.R. Small (formerly J.E. Rudzki).

generated by a reference compound to that of the sample compound of interest. Each waveform is produced when the sample or reference solution absorbs light from the laser pulse and responds by releasing heat, by changing molecular shape or dimensions, or by altering electrical charge (for example, by proton or electron ejection into the solution). All of these processes have the potential for rapidly changing the volume of the irradiated region of the solution. The volume change generates a transient pressure wave measurable by the photoacoustic transducer in contact with the sample cuvette or immersed in the solution. The voltage response of the transducer to the pressure wave is amplified and digitized, giving rise to the photoacoustic waveform, the measured voltage as a function of time.

As shown previously [11], deconvolution analysis of such data gives the magnitude of the signal-inducing event (e.g. heat release or molecular volume change), as well as the rate of that event. Photoacoustic waveform deconvolution programs have been presented by Rudzki Small and co-workers [11], Heihoff and Braslavsky [12], and Melton and co-workers [13]. In this paper, we describe the adaptation and use of a fluorescence nonlinear least squares iterative reconvolution program, utilizing the Marquardt algorithm [14], for photoacoustic waveform deconvolution. The adaptation process required changes in the computer code which are of interest to both the fluorescence and photoacoustic fields. A preliminary version of this program has been described earlier [15], and the final FORTRAN version is available upon request from the authors.

2. Experimental

All measurements were made at room temperature (20–23 °C).

2.1 Materials

Benzophenone (Gold Label), ferrocene and 2,5-dimethyl-2,4-hexadiene were obtained from Aldrich (Milwaukee, WI). The ferrocene was sublimed once before use; all other compounds were used as they were obtained. Reagent grade acetonitrile was used as solvent throughout.

2.2 Photoacoustic measurements

The photoacoustic apparatus is similar to that described previously [16]. Photoexcitation is achieved by the output of a nitrogen laser (PRA LN120C, 300 ps pulse width, 337.1 nm; Laser Photonics, Orlando, FL) operated at a 1 Hz repetition rate. The laser pulse is divided by a beam splitter so that about 9 μJ is incident on the sample cuvette, while about 35 μJ is diverted to an RjP-735 energy meter probe (Laser Precision, Utica, NY). The energy meter (Laser Precision Rj-7620) thus provides a measure proportional to the pulse energy incident on the sample. The sample is contained in a standard, 1-cm pathlength, quartz fluorescence cuvette. A lens (10-cm focal length) is placed 7.5 cm before the front surface of the cuvette to give a beam diameter of about 2 mm, centered side-to-side on the cuvette face.

Volumetric changes induced by photoinitiated events are detected by a V103, 1-MHz, or A125S, 2.25-MHz piezoelectric-element-based transducer (Panametrics, Inc., Waltham, MA), clamped to the side of the cuvette with a layer of silicone grease interfacing the transducer and cuvette. Care is taken not to disturb the cuvette/transducer arrangement while changing samples. The transducer signal is amplified (Panametrics 5676 ultrasonic preamplifier, 0.05–20 MHz, 10^4 gain) and digitized by a Tektronix (Beaverton, OR) 2430 digital oscilloscope. The oscilloscope is operated at 10 ns per point (1024 points total), 20 mV per division (8-bit vertical resolution). Data from 100 laser pulses are averaged to give one photoacoustic waveform. The data are collected and processed by a Tektronix PEP 301 controller using ASYST software.

The linearity of the photoacoustic response with pulse energy is checked in each experiment to avoid saturation and other nonlinear effects. Optical filters are placed at the light output of the laser to attenuate the light such that the incident intensity on the sample may be variable from 9 to 2 μJ per pulse, with concomitant de-

creases in the energy measured by the energy meter probe. When deconvolution of reference and sample waveforms yields consistent results, independent of incident photon energy in the 2 to 9 μJ range, the instrument is said to be operating in a linear range. In general, adjustments of distance from the lens to the cuvette front surface have been found to be useful in optimizing the linearity of the instrument. Changing the position of the lens changes the diameter of the laser beam passing through the cuvette. While a smaller beam diameter increases the photoacoustic signal-to-noise ratio, and theoretically the lifetime resolution of the system [1,2,12], we have found that photon saturation effects caused by small laser beam diameters adversely affect the resolution of kinetic and thermodynamic parameters in the test system of ferrocene (reference compound) and benzophenone (sample compound) in acetonitrile. Thus, our experimental system is best operated with a laser beam diameter of 1–2 mm passing through the cuvette.

The optical densities of the reference and sample compounds are adjusted to be within 10% of each other in order to minimize differences in concentration gradients of heat-producing transients. This is important because the sample absorbance affects not only the amplitude of the photoacoustic waveform, but also the position of the waveform on the time axis relative to laser firing. The latter effect is geometric in origin: for strongly absorbing samples, most of the photoacoustic waveform generation is from the front surface of the cuvette rather than the interior of the cuvette. Solution optical densities between 0.2 and 0.8 are commonly used. The actual absorbances at the excitation wavelength are incorporated into the data analysis by a $(1 - 10^{-A})$ factor (A = absorbance), as described below. We have found that the photoacoustic signal amplitude is linear with $(1-10^{-A})$, so that the $(1 - 10^{-A})$ factor corrects for the dependence of the waveform *amplitude* (but not time-axis *position*) on absorbance.

All samples are degassed by bubbling argon through them for 2 min and maintained under argon atmosphere during data collection. Studies with pyrene have shown that the degassing is essentially complete within 2 min, to the extent achievable by the method. The measurements required for an experiment are: photoacoustic waveforms for the reference and sample compounds; average energy meter readings measured concomitant with those waveforms; absorbances of all of the solutions at 337 nm; and a waveform baseline collected for 100 laser pulses with no laser light incident on the cuvette.

3. Data analysis

Preprocessing of photoacoustic data is necessary before waveform deconvolution is performed. The waveform baseline is subtracted from each photoacoustic waveform to yield a net waveform having positive and negative excursions. As suggested by eq. (4) below and described previously [11], each point of the net waveforms must be divided by the sample absorbance factor $(1 - 10^{-A}$, where A is the absorbance at the excitation wavelength, 337 nm) and by the average laser pulse energy, E_0, as measured by the energy meter. The reference waveform thus processed is then normalized to 1.0 at its maximum amplitude, and the same normalization factor is then applied to the sample waveform. At this stage, the waveforms are ready for deconvolution.

Deconvolution is achieved by an iterative nonlinear least squares technique adapted, as described in this paper, from a time-resolved fluorescence decay computer program utilizing the Marquardt algorithm. Versions of the program are available in both ASYST and FORTRAN languages. The reference waveform is taken to represent the instrument response to fast (< 1 ns), complete, thermally induced volume changes. The sample waveform may represent other processes, with different kinetics. The reference and sample waveforms are input into the computer program, and a portion of the waveforms is selected for analysis. Generally, this includes the first few oscillations, where the signal-to-noise ratio is highest and where there are no contributions from acoustic reflections in the cuvette. The data are deconvolved for one or two simultaneous exponential decays, with the results expressed as τ_i (lifetime) and ϕ_i (preexponential factor) values.

The goodness of fit is judged by reduced χ^2 values, by visual inspection of the residuals, and by the autocorrelation of the residuals. Reduced χ^2 is defined as usual [17] by:

$$\chi^2 = \frac{1}{(n_2 - n_1 + 1) - n_{\text{var}}} \sum_{i=n_1}^{n_2} [C(i) - S(i)]^2, \tag{1}$$

where n_1 and n_2 are, respectively, the starting channel and ending channel of the analysis, n_{var} is the total number of variables being sought (ϕ's and τ's), and $C(i)$ and $S(i)$ are the values of the convolved wave and the sample wave at channel i, respectively. The autocorrelation of the residuals is given by [17]:

$$\text{cor}(j) = \left(\frac{1}{(n_2 - n_1 + 1) - j} \sum_{i=n_1}^{n_2 - j} [C(i) - S(i)] \times [C(i+j) - S(i+j)] \right) \times \left(\frac{1}{(n_2 - n_1 + 1)} \sum_{i=n_1}^{n_2} [C(i) - S(i)]^2 \right)^{-1}, \tag{2}$$

where j is an index which runs from 0 to $(n_2 - n_1 + 1)/2$. A "good" autocorrelation is represented by cor(0) = 1.0, cor(j) = 0.0 for $j \neq 0$.

Simulated data

Photoacoustic waveforms were modeled according to the equation:

$$V(t) = \sum_{i=1}^{n} K' \phi_i \frac{\nu/\tau_i}{\nu^2 + (1/\tau_i')^2} \times \left\{ \exp(-t/\tau_i) - \exp(-t/\tau_0) \times \left[\cos(\nu t) - \frac{1}{\nu \tau_i'} \sin(\nu t) \right] \right\}, \tag{3}$$

where $V(t)$ is the detector response, K' is a constant (taken to be unity), ν is the characteristic oscillation frequency of the transducer, τ_0 is the relaxation time of the transducer, ϕ_i is the amplitude factor for the ith decay, τ_i is the lifetime of the ith decay, t is time, and $1/\tau_i' = 1/\tau_i - 1/\tau_0$. This eq. (3) is the corrected version of eq. (3) in ref. [11], which was missing one set of brackets. The origin of this equation is the *point source / point detector* model of photoacoustic calorimetry developed by Rothberg et al. [18]. We have maintained the original terminology and variables presented in that work. We point out, however, that in this framework, $\nu = 2\pi f$, where f is the frequency of the transducer in Hz. Thus, waveforms simulated with $\nu = 10^6$ rad s^{-1} have an apparent period of 2π μs (see Fig. 1). The factor of 2π has no significant effect on the outcome of either the simulated or experimental data presented herein.

As described previously [11], eq. (3) represents the mathematical convolution of n simultaneous transient decays with a model transducer response function (which may be described by $n = 1$, $\tau_1 \ll 1/\nu$ and $\tau_1 \ll \tau_0$). Equation (3) may be used to simulate reference and sample waveforms of known ϕ_i and τ_i values. The waveforms may then be deconvolved using the modified Marquardt program described in this paper.

Simulated noise was added to waveforms by a computer program which computes a normally-distributed random number with a given mean (the original, noiseless data point) and standard deviation (specified by the user), and thus generates a new, noisy waveform based on the original noiseless data.

4. Theory

In general, the measured photoacoustic voltage signal with time and temperature, $V(t, T)$, is given by

$$V(t, T) = k \sum_i \left\{ \phi_i \frac{\beta(T)}{C_p \rho} + \frac{m_i}{h\nu} \right\} E_0 (1 - 10^{-A}) \times M(t) * q_i(t), \tag{4}$$

where the variables are as follows (common units are in brackets):

i is the index for the transient decay of interest;

ϕ_i is the fraction of photon energy released as heat for the ith transient decay;

$\beta(T)$ is the thermal volumetric expansion coefficient of the solvent [K^{-1}] (for water, $\beta(T)$ is strongly dependent on temperature);

T is the temperature [K];

C_p is the specific heat of solvent at constant pressure [cal g^{-1} K^{-1}];

ρ is the solvent density [g L^{-1}];

m_i is the volume change per mole of photoexcited molecules for the ith decay [L mol^{-1}];

$h\nu$ is the photon energy [cal mol^{-1}];

E_0 is the laser pulse energy [cal];

A is the sample absorbance at the photon frequency ν;

t denotes the time [s];

$M(t)$ is the instrumental response, determined primarily by characteristics of the transducer;

$q_i(t)$ is the time-dependent impulse response function, usually involving τ_i variables, with τ_i being the characteristic relaxation time of the ith decay;

k is the proportionality constant relating $V(t, T)$ to the transient volume changes in solution [V L^{-1}]; dependent on instrumental design.

In addition, the asterisk (*) denotes a convolution integral:

$$M(t) * q_i(t) = \int_0^t M(u)\, q_i(t-u)\, \mathrm{d}u. \qquad (5)$$

The form of $q_i(t)$ cannot be determined *a priori*, and a choice of model must be made based on what is expected theoretically. Two models which are commonly encountered for photoacoustic applications are simultaneous exponential decays, i.e. $q_i(t) = (1/\tau_i)\ \exp(-t/\tau_i)$, and sequential exponential decays (also characterized by a sum of exponentials) [11].

For the data presented in this paper, the photoacoustic signals are assumed to derive from heat release only, with no contributions from photoinduced volume changes. Thus, a reported preexponential factor may be interpreted as a ϕ_i value, the fraction of the photon energy released as heat in the ith exponential decay.

Let R and S represent $V(t, T)$ for the reference and sample, respectively. Both waveforms are governed by eq. (4). Care must be taken to measure R and S under identical experimental geometry (i.e., same k), solvent conditions (i.e., same $\beta(T)$, C_p and ρ), and temperature, T. The sample absorbance, A, and incident laser pulse energy, E_0, should be similar; however, small differences in A and E_0 for the sample and reference waveforms may be corrected for mathematically. The reference compound is chosen to be one which relaxes back to the ground state (lifetime τ) with unit efficiency on a timescale very fast compared to the transducer response (frequency ν_{tr}). This feature means that, for a reference compound, the $M(t) * q_i(t)$ term in eq. (4) is indistinguishable from $M(t)$:

$$M(t) * q_i(t) = M(t) \quad \text{for} \quad \tau_i \ll 1/\nu_{\mathrm{tr}}. \qquad (6)$$

Note that this feature reduces the convolution in eq. (4) to a simple multiplication, from which the instrumental response, $M(t)$, can be calculated. Then:

$$M(t) = R(t)/k', \qquad (7)$$

where k' is a constant under the conditions of identical k, $\beta(T)$, C_p, ρ, A, and E_0 for the R and S waveforms, and m_i is taken to be zero for this discussion. It follows that:

$$S(t) = k' \sum_i \phi_i\, M(t) * q_i(t)$$

$$= \sum_i \phi_i\, R(t) * q_i(t). \qquad (8)$$

In principle, then, the sample waveform S may be deconvolved using the reference waveform R to yield the desired parameters, ϕ_i and τ_i.

By defining the function $h(t)$ as:

$$h(t) = \sum_i \phi_i\, q_i(t) = \sum_i \phi_i (1/\tau_i)\ \exp(-t/\tau_i), \qquad (9)$$

where the expression given is for simultaneous exponential decays, then eq. (8) becomes:

$$S(t) = R(t) * h(t). \qquad (10)$$

This equation is equivalent to the expression

$C_{\text{exptl}}(t) = E(t) * T(t)$ described earlier [11], with $C_{\text{exptl}}(t)$, $T(t)$ and $E(t)$ equivalent to $S(t)$, $R(t)$ and $h(t)$, respectively.

4.1 Quadratic-fit convolution program

The derivations of the equations utilized for modifying the original Marquardt program for photoacoustic waveform analysis are given below. For clarity, the ϕ preexponential factor, a simple constant in the convolution expression, has not been included in the following equations.

4.1.1 Extension of the convolution to a later time

Given $C(a) = \int_0^a R(u)(1/\tau)\, e^{-(a-u)/\tau}\, du$, calculate $C(b)$ for $b > a$ in terms of $C(a)$ and the convolution on $R(u)$ over the time interval from a to b.

$$C(b) = \int_0^b R(u)\frac{1}{\tau}e^{-(b-u)/\tau}\, du$$
$$= \frac{1}{\tau}e^{-b/\tau}\left\{\int_0^a R(u)\, e^{u/\tau}\, du + \int_a^b R(u)\, e^{u/\tau}\, du\right\}.$$

Letting $\Delta = b - a$ and $v = u - a$:

$$C(b) = e^{-\Delta/\tau}C(a) + \int_0^\Delta R(a+v)\frac{1}{\tau}e^{-(\Delta-v)/\tau}\, dv. \qquad (11)$$

The second term is the convolution of $R(u)$ from $u = a$ to $u = a + \Delta = b$, with the 0 of time shifted to a. This is the desired result. It says that $C(b)$ is the sum of $C(a)$ after decaying for the time period Δ, plus the separate convolution of the exponential with $R(u)$ in the a to b interval.

4.1.2 Convolution result using the quadratic-fit approximation

$R(u)$ is represented by a series of numbers (R_n, photoacoustic wave amplitude at channel n) evenly spaced on the time axis by the interval δ. We might assume that the value of $R(u)$ between points is equal to the value of the following point ("square wave" approximation), or that the value of $R(u)$ between points is given by a linear interpolation ("linear interpolation" approximation). Instead, for the purposes of integration, we assume that the value of $R(u)$ between points R_n and R_{n+2} is given by a quadratic which passes through the three points (including R_{n+1}):

$$R(v) = \frac{R_n - 2R_{n+1} + R_{n+2}}{2\delta^2}v^2 + \frac{-\frac{3}{2}R_n + 2R_{n+1} - \frac{1}{2}R_{n+2}}{\delta}v + R_n$$
$$= Av^2 + Bv + C, \quad \text{with } (n+1)\delta \geqslant u \geqslant n\delta,$$
$$v = u - n\delta.$$

(This equation may be verified by simply replacing v by 0, δ, and 2δ to give $R(v) = R_n$, R_{n+1} and R_{n+2}, respectively.)

Given the convolution to point n (C_n), the object is to calculate the value of the convolution at point $n+1$ (C_{n+1}) and $n+2$ (C_{n+2}). From the result in part A, with $a = n\delta$ and $b = (n+1)\delta$, we can write:

$$C_{n+1} = C_n\, e^{-\delta/\tau} + R_n\left[-e^{-\delta/\tau} + \tfrac{1}{2}(1 - 3\, e^{-\delta/\tau})(\tau/\delta) + (1 - e^{-\delta/\tau})(\tau/\delta)^2\right] + R_{n+1}\left[1 + 2\, e^{-\delta/\tau}(\tau/\delta) - 2(1 - e^{-\delta/\tau})(\tau/\delta)^2\right] + R_{n+2}\left[-\tfrac{1}{2}(1 + e^{-\delta/\tau})(\tau/\delta) + (1 - e^{-\delta/\tau})(\tau/\delta)^2\right]. \qquad (12)$$

Also, with $a = n\delta$ and $b = (n+2)\delta$:

$$C_{n+2} = C_n\, e^{-2\delta/\tau} + R_n\left[-e^{-2\delta/\tau} - \tfrac{1}{2}(1 + 3\, e^{-2\delta/\tau})(\tau/\delta) + (1 - e^{-2\delta/\tau})(\tau/\delta)^2\right] + R_{n+1}\left[2(1 + e^{-2\delta/\tau})(\tau/\delta) - 2(1 - e^{-2\delta/\tau})(\tau/\delta)^2\right] + R_{n+2}\left[1 - \tfrac{1}{2}(3 + e^{-2\delta/\tau})(\tau/\delta) + (1 - e^{-2\delta/\tau})(\tau/\delta)^2\right]. \qquad (13)$$

These are the required results. As a starting procedure it is necessary to note only that $C_0 = 0$ and $R_0 = 0$. Note also that, as $\tau \to 0$, $C_{n+1} \to R_{n+1}$ and $C_{n+2} \to R_{n+2}$, as expected.

4.1.3 Derivatives required for Marquardt algorithm

In order to make changes to the original Marquardt program, the following derivatives with respect to τ are necessary:

$$\begin{aligned}\partial C_{n+1}/\partial\tau = {} & C_n(\delta/\tau^2)\,\mathrm{e}^{-\delta/\tau} + R_n\big[1/2\delta + 2\tau/\delta^2 \\ & + (-5/2\delta - 2\tau/\delta^2 \\ & - 3/2\tau - \delta/\tau^2)\,\mathrm{e}^{\delta/\tau}\big] \\ & + R_{n+1}\big[-4\tau/\delta^2 + (4/\delta \\ & + 4\tau/\delta^2 + 2/\tau)\,\mathrm{e}^{-\delta/\tau}\big] \\ & + R_{n+2}\big[-1/2\delta + 2\tau/\delta^2 \\ & + (-3/2\delta - 2\tau/\delta^2 - 1/\tau)\,\mathrm{e}^{-\delta/\tau}\big]; \end{aligned} \tag{14}$$

$$\begin{aligned}\partial C_{n+2}/\partial\tau = {} & C_n(2\delta/\tau^2)\,\mathrm{e}^{-2\delta/\tau} \\ & + R_n\big[-1/2\delta + 2\tau/\delta^2 + (-7/2\delta \\ & - 2\tau/\delta^2 - 3/\tau - 2\delta/\tau^2)\,\mathrm{e}^{-2\delta/\tau}\big] \\ & + R_{n+1}\big[2/\delta - 4\tau/\delta^2 \\ & + (6/\delta + 4\tau/\delta^2 + 4/\tau)\,\mathrm{e}^{-2\delta/\tau}\big] \\ & + R_{n+2}\big[-3/2\delta + 2\tau/\delta^2 \\ & + (-5/2\delta - 2\tau/\delta^2 - 1/\tau)\,\mathrm{e}^{-2\delta/\tau}\big]. \end{aligned} \tag{15}$$

Incorporation of the preexponential factor, ϕ, is done by multiplying eqs. (12)–(15) through by ϕ. Thus, for the purposes of the Marquardt algorithm [14], the required derivatives with respect to ϕ will be simply C_{n+1} and C_{n+2}. Equations (12)–(15) were substituted into the original Marquardt program utilized for fluorescence analysis. The program was modified to prevent any value of τ from becoming negative; τ is constrained to be greater than or equal to 1 fs. No changes were made in the α and β matrices [14], so that the methods for minimizing χ^2 were unchanged.

4.2 Extension of the method to sequential decays

In the quadratic-fit convolution program, simultaneous decays are assumed, with $q_i(t) = (1/\tau_i)\,\exp(-t/\tau_i)$ for decay i, $i = 1, 2, 3, \ldots$. What if the decays are sequential rather than simultaneous?

$$\mathrm{A}^* \xrightarrow{\tau_1} \mathrm{B} \xrightarrow{\tau_2} \mathrm{C} \xrightarrow{\tau_3} \mathrm{D} \ldots$$

It can be shown that:

$$q_1(t) = \frac{1}{\tau_1}\exp(-t/\tau_1), \tag{16}$$

$$q_2(t) = \frac{1}{\tau_1 - \tau_2}\big[\exp(-t/\tau_1) - \exp(-t/\tau_2)\big], \tag{17}$$

$$\begin{aligned} q_3(t) = {} & \frac{\tau_1}{(\tau_1 - \tau_3)(\tau_1 - \tau_2)}\exp(-t/\tau_1) \\ & - \frac{\tau_2}{(\tau_1 - \tau_2)(\tau_2 - \tau_3)}\exp(-t/\tau_2) \\ & + \frac{\tau_3}{(\tau_1 - \tau_3)(\tau_2 - \tau_3)}\exp(-t/\tau_3). \end{aligned} \tag{18}$$

Note that the number of exponentials required will equal the number of reactions in the sequence. For a two-step sequential process, only eqs. (16) and (17) are required.

It is apparent that the sums of the $q_i(t)$ will be sums of exponentials and, thus, analyses of data arising from sequential decays can still be done with the quadratic-fit convolution program. In principle, the correct τ values will be returned regardless of which kinetic model, simultaneous or sequential, is valid. However, interpretation of the preexponential factors obtained will depend on the model assumed. For example, given a three-component fit by the analysis program and assuming a three-step sequential process, one may write:

$$\phi_1^{\mathrm{app}} = \phi_1 + \phi_2\frac{\tau_1}{\tau_1 - \tau_2} + \phi_3\frac{\tau_1^2}{(\tau_1 - \tau_2)(\tau_1 - \tau_3)}, \tag{19}$$

$$\phi_2^{\mathrm{app}} = \phi_2\frac{\tau_2}{\tau_2 - \tau_1} + \phi_3\frac{\tau_2^2}{(\tau_2 - \tau_1)(\tau_2 - \tau_3)}, \tag{20}$$

$$\phi_3^{\text{app}} = \phi_3 \frac{\tau_3^2}{(\tau_1 - \tau_3)(\tau_2 - \tau_3)}, \tag{21}$$

where ϕ_i^{app} are the amplitude values reported by the quadratic-fit convolution program for the exponential decays. (In the case of only two sequential exponential decays, ϕ_3 may be set to zero.) The ϕ_i values for the sequential decays can be obtained by solving the simultaneous equations:

$$\phi_3 = \phi_3^{\text{app}} \frac{(\tau_3 - \tau_1)(\tau_3 - \tau_2)}{\tau_3^2}, \tag{22}$$

$$\phi_2 = \phi_2^{\text{app}} \frac{\tau_2 - \tau_1}{\tau_2} + \phi_3 \frac{\tau_2}{\tau_3 - \tau_2}, \tag{23}$$

$$\phi_1 = \phi_1^{\text{app}} + \phi_2 \frac{\tau_1}{\tau_2 - \tau_1} + \phi_3 \frac{\tau_1^2}{(\tau_3 - \tau_1)(\tau_1 - \tau_2)}. \tag{24}$$

It is apparent from these equations that if τ_1, τ_2, and τ_3 are well separated (e.g., $\tau_1 = 1$ ns, $\tau_2 = 1$ μs, and $\tau_3 = 1$ ms), then the apparent ϕ values are equivalent to the actual ϕ values.

5. Results

The quadratic-fit convolution program was tested with simulated waveform data, to which varying levels of noise were added, as well as with experimental data obtained using two commercially available transducers.

5.1 Simulated data

Figure 1 shows three typical modeled waveforms with varying levels of Gaussian noise added to them. All were modeled assuming one transient decay using eq. (3), with $\nu = 10^6$ rad s^{-1} and $\tau_0 = 1$ ms, comparable to the model studies done previously [11]. As described previously [11], curve a would appear the same for any lifetime less than 1 ns; longer decay lifetimes diminish the maximum waveform amplitude and spread the function to longer times.

A typical data analysis problem is shown in Fig. 2, using synthetic waveforms to which 0.01

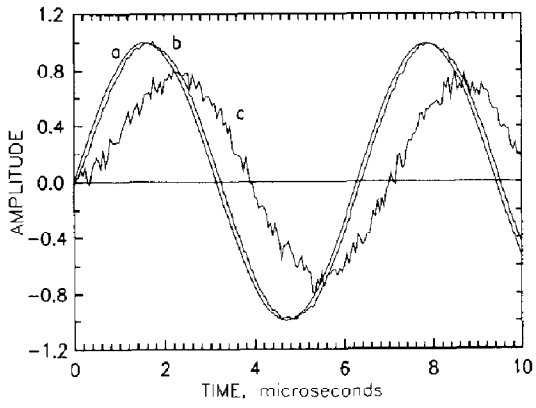

Fig. 1. Examples of simulated photoacoustic waveforms to which various levels of Gaussian noise have been added. The waveforms were generated using eq. (3) in the text, with $\phi = 1.0$ and $\tau = 1$ ns (a), 100 ns (b), or 1 μs (c). The added noise levels are (a) none, (b) 0.01 standard deviation and (c) 0.05 standard deviation.

standard deviation of Gaussian noise has been added. This noise level is slightly higher than that commonly seen in our experimental data. In Fig. 2(A), the reference waveform (curve a) was generated using eq. (3) with $\phi = 1.0$ and $\tau = 1$ fs, while the sample waveform (curve b) was generated as a two-component decay, $\phi_1 = \phi_2 = 0.5$, $\tau_1 = 1$ ns and $\tau_2 = 1$ μs. In this case, the analysis was done with the finished version of the modified analysis program. The starting guesses were $\phi_1 = \phi_2 = 1.0$, $\tau_1 = 0.1$ ns and $\tau_2 = 100$ ns, with no fixed variables. The final fit is shown by curve (c), in which the recovered parameters are $\phi_1 = 0.502$, $\tau_1 < 50$ ns, $\phi_2 = 0.502$, and $\tau_2 = 1.01$ μs. Figure 2(B) shows the residuals of the analysis, and Fig. 2(C) shows the autocorrelation of the residuals, both indicating an acceptable fit.

The original Marquardt computer program, as used for fluorescence decay analysis, failed to accurately analyze photoacoustic data, even without added noise, when the τ value was less than the digitization channel width. This is shown in Table 1 for data modeled using a 50 ns digitization channel width. While the recovered ϕ and τ values for modeled τ values greater than 50 ns are accurate, those for modeled τ values less than 50 ns are substantially inaccurate. This was the incentive for modifying the numerical convolution algorithm of the original Marquardt pro-

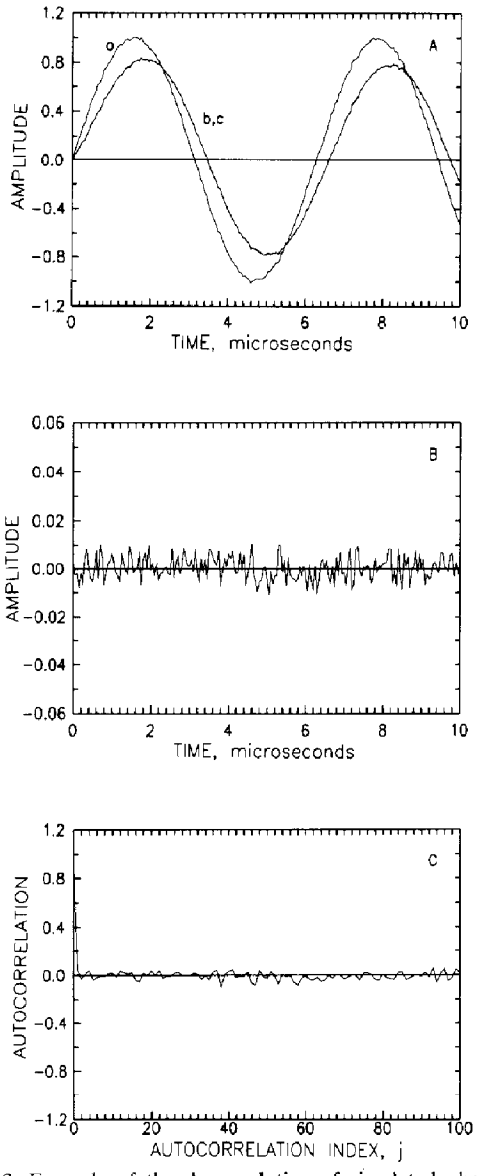

Fig. 2. Example of the deconvolution of simulated photoacoustic waveforms. (A) The reference waveform (a) and sample waveform (b) were simulated using eq. (3) in the text. Gaussian noise (0.01 standard deviation) was added to curves (a) and (b). This system was analyzed by the final form of the quadratic-fit convolution computer program described in the text. The best fitting curve returned by the computer program is curve (c), which is the convolution of the reference waveform with two simultaneous exponential decays. (B). The residuals of the fit in (A), expressed as curve (c) minus curve (b). (C). The autocorrelation of the residuals in (B). The autocorrelation function is described by eq. (2) in the text.

gram. A successful analysis program for photoacoustic data should accurately report both ϕ and τ values for lifetimes longer than the channel width. For a lifetime shorter than the channel width, the program should report the correct ϕ value, as well as a τ value which is less than the channel width. The data in Table 1 show that the quadratic-fit convolution program is successful for noiseless, single-component data. All of the data analyses reported hereafter were done with the quadratic-fit convolution program.

The effect of added noise on the recovery of modeled parameters is shown in Fig. 3, which presents the results from analyses of photoacoustic waveforms generated using single exponential decays. The reference waveform was modeled with a fs decay lifetime, while the sample decay lifetime ranged from 10 ns to 100 μs. In general, for noiseless data, the recovered ϕ and τ values closely agree with the modeled values, as seen by the horizontal lines (with square symbols) in Figs. 3(A) and (B). The curves for 0.01 and 0.05 standard deviation added noise show less perfect recovery of the modeled parameters. For modeled τ values less than the 50 ns digitization channel width, the recovered lifetimes were sometimes greater (e.g., for the 0.05 standard deviation noise) or less (0.01 standard deviation noise) than the true values (Fig. 3A). However, all of those recovered lifetimes were less than the channel width, indicating a fast decay. More im-

Table 1

Recovery of ϕ and τ parameters from the original Marquardt computer program in comparison with those from the version modified for photoacoustic waveform analysis

Modeled [a]		Recovered			
		Original program		Modified program	
ϕ	τ	ϕ	τ	ϕ	τ
1.0	1 ns	0.557	9.46 ns	1.00	0.998 ns
1.0	10 ns	0.850	17.6 ns	1.00	9.99 ns
1.0	50 ns	0.995	50.9 ns	1.00	50.0 ns
1.0	100 ns	1.00	100 ns	1.00	100 ns
1.0	1 μs	1.00	1.00 μs	1.00	1.00 μs
1.0	10 μs	1.00	10.0 μs	1.00	10.0 μs
1.0	100 μs	1.00	100 μs	1.00	100 μs

[a] Modeling was done using eq. (3) in the text, with $\nu = 10^6$ rad s^{-1}, $\tau_0 = 1$ ms, and with time sampling done every 50 ns. The reference waveform was generated with $\phi = 1.0$, $\tau = 1$ fs. The sample waveform was generated using the values listed. All data are without added synthetic noise.

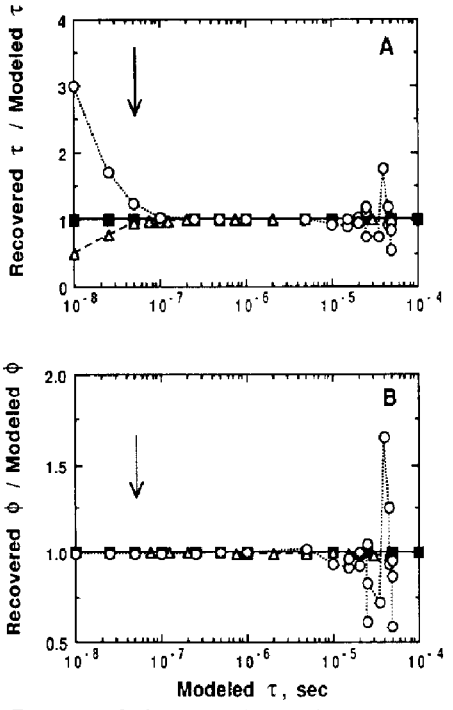

Fig. 3. Recovery of photoacoustic waveform parameters for single exponential decays with varying levels of noise. The waveforms were simulated using eq. (3) in the text, with $\nu = 10^6$ rad s^{-1}, $\tau_0 = 1$ ms, and a 50 ns per point sampling interval. The reference waveforms were generated with $\phi = 1.0$ and $\tau = 1$ fs, while the sample waveforms were generated with $\phi = 1.0$ or 0.5 and τ = variable from 10 ns to 100 μs (reported as the *X*-axis variable). The *Y*-axis values are the recovered τ (A) or ϕ (B) parameters, divided by the values used to generate the data. Thus, a *Y*-axis value of 1.0 indicates good recovery of the modeled parameter. For both (A) and (B), the solid, dashed and dotted lines (with square, triangle and circle symbols) represent 0.00, 0.01 and 0.05 standard deviation of Gaussian noise, respectively, added to the reference and sample waveforms. The arrows indicate the time value of 50 ns, which was the sampling interval for the simulations. The starting guesses were $\phi = 1.0$ and $\tau = 20$ or 100 ns.

portant from the photoacoustics point of view, the recovered ϕ values were unaffected by the noise level for such fast decays (Fig. 3B).

The 0.05 standard deviation data in Fig. 3(A) show considerable scatter about the modeled τ values for large τ, e.g. 10^{-5} to 10^{-4} s. This is also true for the recovered ϕ data in Fig. 3(B). The reason for this is that the amplitude of the waveform oscillations has dropped to or below the magnitude of the added noise. The true data are thus "lost in the noise", and there is considerable uncertainty in the recovered parameters.

The next consideration is the recovery of data from waveforms generated from two simultaneous exponential decays. The first criterion for distinguishing a two-component decay from a one-component decay is the reduction in χ^2 which occurs upon allowing a second component in the least squares analysis. For noiseless two-component data, indicated by the squares in Fig. 4(A), there is a substantial decrease in χ^2 in going from one-component (open squares) to two-component (solid squares) analyses. The exception is in the region of $\tau_1 = \tau_2 = 1$ μs, where the χ^2 values coincide. Similar results are seen for 0.01 and 0.05 standard deviation added noise

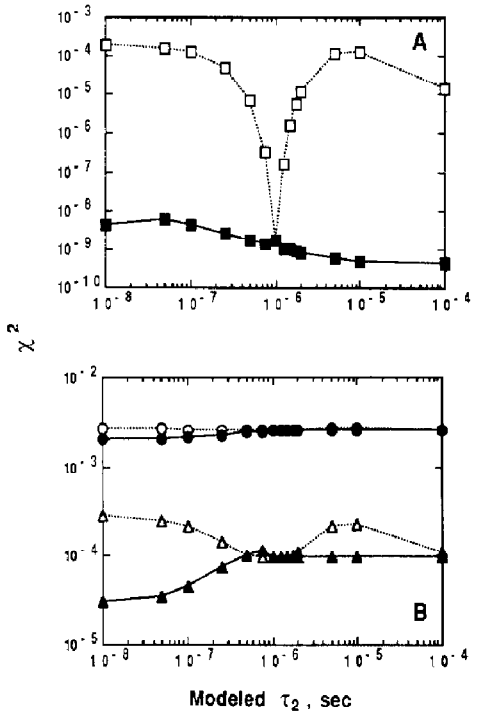

Fig. 4. Ability to resolve two decay components from simulated waveforms with varying levels of added noise. The waveforms were simulated using eq. (3) in the text, with $\nu = 10^6$ rad s^{-1}, $\tau_0 = 1$ ms, and a 50 ns per point sampling interval. The reference waveforms were generated with $\phi = 1.0$ and $\tau = 1$ fs, while the sample waveforms were generated with $\phi_1 = \phi_2 = 0.5$, $\tau_1 = 1$ μs and τ_2 = variable (reported as the *X*-axis variable). The *Y*-axis values are the χ^2 values recovered for one-component (*open* symbols) and two-component (*filled* symbols) analyses. Shown are the results for analyses of waveforms with no noise (squares, part A), and 0.01 and 0.05 standard deviation of Gaussian noise (triangles and circles, respectively; part B) added to the reference and sample waveforms.

data (Fig. 4B; triangles and circles, respectively), except that the reduction in χ^2 in going from one-component (open symbols) to two-component (solid symbols) analyses is less dramatic, and the higher χ^2 values reflect the noise levels. The data with moderate added noise (0.01 standard deviation, Fig. 4B), reflecting typical experimental data, suggest that for a τ_1 of 1 μs, τ_2 must be less than 0.5 τ_1 or greater than 2 τ_1 for adequate indication that two components are present. While not shown here, the residuals and autocorrelation function should also be used to judge the acceptability of an analysis [17].

Table 2 presents the results of four two-component resolutions, each with three levels of added noise. In all cases, the recovered parameters are very close to the modeled parameters for noiseless data. In addition, for the first data set, the modeled τ values of 1 ns and 1 μs are well separated, and the recovered parameters are very close to the modeled parameters for all added noise levels.

The other results in Table 2 are for somewhat difficult two-component resolutions. For the second data set, $\tau_1 = 1$ ns and $\tau_2 = 100$ ns, the resolution is difficult in that the digitization channal width of 50 ns is comparable to the longer 100 ns decay time. Even at the 0.01 standard deviation noise level the ϕ and τ values recovered are considerably different than the true values. However, note that the χ^2 values obtained clearly suggest that more than one component is present, even at the 0.05 standard deviation noise level. For the third data set in Table 2, that of 100 ns and 1 μs, only a factor of 10 separates the two lifetimes. However, at both noise levels, resolution of the two decays is attained with reasonable accuracy. Finally, the last data set shows the recovery of values for 1 and 10 μs modeled decays. For 0.00 and 0.01 standard deviation added noise, the recovered results are excellent, while for the 0.05 standard deviation added noise data, not only is resolution not achieved but also the very low ratio of $\chi_1^2/\chi_2^2 = 1.03$ is insufficient to suggest that more than one component is present. Once again, the information on the 10 μs component appears to have been masked by the noise due to the inherently small oscillation amplitude for slow decay components. However, the 10 μs component is being detected since the

Table 2

Recovery of ϕ and τ parameters from simultaneous two-component photoacoustic waveforms as a function of added noise level

Modeled [a] ($\phi_1 = \phi_2 = 0.5$)		Added noise (Stand. Dev.)	χ_1^2/χ_2^2 [b]	Recovered				
τ_1	τ_2			ϕ_1	τ_1 [c]	ϕ_2	τ_2	$\phi_1 + \phi_2$
1 ns	1 μs	0.00	$>10^3$	0.50	< 50 ns	0.50	1.0 μs	1.0
		0.01	10	0.50	< 50 ns	0.51	1.0 μs	1.0
		0.05	1.1	0.51	< 50 ns	0.56	1.2 μs	1.1
1 ns	0.1 μs	0.00	400	0.52	< 50 ns	0.48	0.10 μs	1.0
		0.01	10	0.81	< 50 ns	0.20	0.28 μs	1.0
		0.05	1.2	0.86	< 50 ns	0.15	0.37 μs	1.0
0.1 μs	1 μs	0.00	$>10^3$	0.50	0.10 μs	0.50	1.0 μs	1.0
		0.01	5	0.40	< 50 ns	0.61	0.87 μs	1.0
		0.05	1.2	0.52	< 50 ns	0.62	1.4 μs	1.1
1 μs	10 μs	0.00	$>10^3$	0.50	1.0 μs	0.50	10 μs	1.0
		0.01	2	0.50	0.99 μs	0.50	9.7 μs	1.0
		0.05	1.03	0.08	< 50 ns	0.70	1.7 μs	0.78

[a] Modeling was done using eq. (3) in the text, with $\nu = 10^6$ rad s^{-1}, $\tau_0 = 1$ ms, and with time sampling done every 50 ns. The reference waveform was generated with $\phi = 1.0$, $\tau = 1$ fs. The sample waveform was generated using the values listed.

[b] The ratio of unweighted χ^2 for a single component analysis to that for a two-component analysis.

[c] Recovered values less than the 50 ns channel width are reported only as < 50 ns.

predominant lifetime recovered, 1.7 μs, is intermediate between the 1 and 10 μs modeled. Table 2 thus shows as expected, that high noise levels can significantly hamper the ability of the quadratic-fit convolution program to resolve closely spaced lifetime pairs, but that some relatively difficult two-component resolutions are possible when only moderate levels of noise are present.

5.2 Transducer comparison using experimental data

Two commercially available transducers were compared in this study. The A125S transducer is described by Panametrics, Inc. as a high-sensitivity, narrowband, tuned transducer, while the V103 transducer is described as an untuned, broadband transducer which provides heavily damped, broadband performance. When used for photoacoustic detection, the transducers give rise to waveforms as shown in Fig. 5. For comparison, curve (a) represents the reference waveform for both the A125S, 2.25-MHz transducer (Fig. 5A) and the V103, 1-MHz transducer (Fig. 5B). It is apparent from Fig. 5 that the A125S transducer is characterized by a higher intrinsic frequency than the V103, and that the V103 is much more highly damped (shows many fewer oscillations) than the A125S transducer. We have found that the two transducers show comparable sensitivity to the magnitude of fast (< 10 ns) heat decays, with the V103 slightly less sensitive.

The quenching of the triplet state of benzophenone (Bph) by 2,5-dimethyl-2,4-hexadiene (DMH) in acetonitrile was studied to determine the response of the transducers to the heat generated by the photoinduced reactions, and to test the quadratic-fit convolution program with experimental data. The quenching of benzophenone by DMH has been successfully measured previously using pulsed-laser photoacoustics with a home-built transducer [11]. The reactions of interest are as follows. Photoexcitation of benzophenone results in the rapid formation (< 6 ps) of the n–π^* triplet state, T_1, with unit efficiency [19]. The benzophenone triplet can undergo triplet-triplet energy transfer with suitable quenchers. This process generates the triplet state of the quencher,

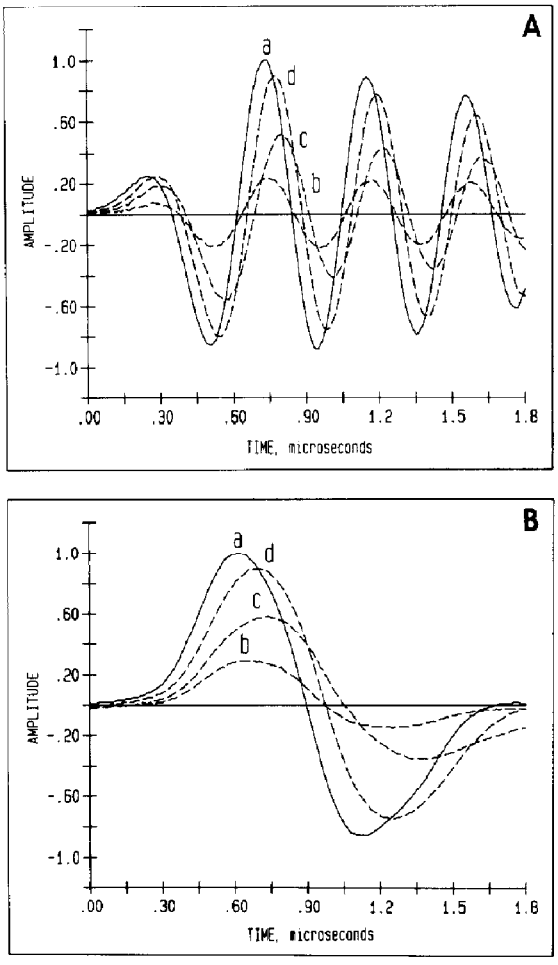

Fig. 5. Photoacoustic waveforms generated using Panametrics (A) A125S, 2.25-MHz and (B) V103, 1.0-MHz transducers. In both (A) and (B), curve (a) represents the reference waveform, generated from ferrocene in acetonitrile. The remaining curves were generated from benzophenone in acetonitrile with varying amounts of 2,5-dimethyl-2,4-hexadiene. In part (A), curves (b), (c) and (d) represent 0.0, 1.0 and 10.0 mM diene, while in part (B), curves (b), (c) and (d) represent 0.0, 0.2 and 1.0 mM diene. All solution absorbances were 0.2 at 337 nm.

^{3}Q, which can then decay to its ground state. Thus, the reaction $T_1 + Q \rightarrow Bph + {}^3Q$ is followed sequentially by the decay of the triplet quencher, $^3Q \rightarrow Q$. In the case of DMH, the triplet lifetime is known to be 44 ± 4 ns [20], and the triplet energy is ~ 59 kcal/mol above ground state [21]. The reference compound for the photoacoustic analysis is ferrocene in acetonitrile, which is known to give rise to a suitable reference waveform [22].

Table 3

Recovered deconvolution parameters for the quenching of triplet benzophenone by 2,5-dimethyl-2,4-hexadiene (DMH) in acetonitrile, measured using the A125S, 2.25-MHz transducer [a]

[DMH] (mM)	ϕ_1^{app}	τ_1 [b]	ϕ_2^{app}	τ_2	ϕ_1	ϕ_2	$\phi_1+\phi_2$
0.00	0.23	< 10 ns	[c]	[c]	0.23	[c]	0.23
0.01	0.24	< 10 ns	[c]	[c]	0.24	[c]	0.24
0.10	0.22	< 10 ns	[c]	[c]	0.22	[c]	0.22
0.20	0.21	< 10 ns	[c]	[c]	0.21	[c]	0.21
0.33	0.20	< 10 ns	1.10	0.45 μs	0.20	1.10	1.30
1.00	0.10	< 10 ns	1.01	0.14 μs	0.11	1.00	1.11
2.00	1.11	85 ns	[d]	[d]	1.11	[d]	1.11
10.0	1.00	39 ns	[d]	[d]	1.00	[d]	1.00

[a] The data were analyzed assuming simultaneous exponential decays, yielding the ϕ_i^{app} values, which were then converted to values appropriate for sequential exponential decays (the ϕ_i values). The conversion method is outlined in the Theory (eqs. 22–24). All reported values are the mean of 3 to 5 determinations; the standard deviation was $\pm 10\%$.

[b] For values of τ_1 of less than 10 ns (the digitization channel width), a value of 1 ns was assumed for converting the ϕ_i^{app} values (for the simultaneous decay analysis) to the ϕ_i values (for sequential decays).

[c] A second component was apparent, but not well-resolved.

[d] There was no resolvable second component.

The relative sensitivity of the transducers to heat depositions of different rates was examined using solutions of benzophenone and the diene quencher DMH. By varying the concentration of DMH, a variety of heat deposition rates can be obtained, and the results may be interpreted by Stern–Volmer analysis [11,19]. The photoacoustic waveform data for solutions of benzophenone and DMH ([DMH] = 0 to 10 mM), as well as for the reference compound ferrocene, were deconvolved using the quadratic-fit convolution program, and the results are presented in Tables 3 and 4. For all of the results reported here, all of the parameters (ϕ_i^{app}, τ_i) were allowed to vary

Table 4

Recovered deconvolution parameters for the quenching of triplet benzophenone by 2,5-dimethyl-2,4-hexadiene (DMH) in acetonitrile, measured using the V103, 1.0-MHz transducer [a]

[DMH] (mM)	ϕ_1^{app}	τ_1 [b]	ϕ_2^{app}	τ_2	ϕ_1	ϕ_2	$\phi_1+\phi_2$
0.00	0.20	< 10 ns	0.37	1.7 μs	0.20	0.37	0.57
0.01	0.20	< 10 ns	0.38	1.5 μs	0.20	0.38	0.58
0.10	0.18	< 10 ns	0.77	0.68 μs	0.18	0.77	0.95
0.20	0.19	< 10 ns	0.87	0.46 μs	0.19	0.87	1.06
0.33	0.22	< 10 ns	0.85	0.31 μs	0.22	0.85	1.07
1.00	0.17	< 10 ns	0.88	0.12 μs	0.18	0.87	1.05
2.00	0.18	< 10 ns	0.91	71 ns	0.19	0.90	1.09
10.0	1.04	32 ns	[c]	[c]	1.04	[c]	1.04

[a] The data were analyzed assuming simultaneous exponential decays, yielding the ϕ_i^{app} values, which were then converted to values appropriate for sequential exponential decays (the ϕ_i values). The conversion method is outlined in the Theory. All reported values are the mean of 3 to 5 determinations, the standard deviation was $\pm 10\%$.

[b] For values of τ_1 of less than 10 ns (the digitization channel width), a value of 1 ns was assumed for converting the ϕ_i^{app} values (for the simultaneous decay analysis) to the ϕ_i values (for sequential decays).

[c] There was no resolvable second component.

freely during the course of the analysis. A sample deconvolution is shown in Fig. 6, with one- and two-component fits of the data. No more than two components were resolvable for any of the data sets. The quadratic-fit convolution program is designed to analyze simultaneous exponential decays, but, as explained in the Theory section, the results may be interpreted in terms of sequential exponential decays. The conversion from simultaneous to sequential kinetics affects only ϕ values, not τ values. The series of reactions of the quenching of benzophenone by DMH is best described by sequential kinetics. Thus, in Tables 3 and 4, the output of the quadratic-fit convolution program is given by ϕ_i^{app} and τ_i, with the corrected ϕ values for sequential kinetics given by ϕ_i. In order to do the conversion of ϕ_i^{app} to ϕ_i, values of τ_i must be used (see Theory). This presents a problem when τ_1 is less than the channel width, which was the case for some of the data in Tables 3 and 4. A decision must be made as to what value to use, since different values of τ_1 will yield different ϕ_i values in the conversion process. In general, the closer τ_1 is to τ_2, the more the change in ϕ_i from ϕ_i^{app}. (For example, in Table 4, the data for 2.0 mM DMH include $\tau_1 < 10$ ns, $\tau_2 = 71$ ns. If τ_1 is chosen as 10 ns, then $\phi_1^{app} = 0.18$ is converted to $\phi_1 = 0.31$. On the other hand, if τ_1 is chosen as 1 ns, then $\phi_1^{app} = 0.18$ is converted to $\phi_1 = 0.19$, a much smaller change.) For the data in Tables 3 and 4, τ_1 is expected to represent the formation of triplet benzophenone, which occurs in < 6 ps from photoexcitation of benzophenone. Thus, choosing a τ_1 value of the resolution limit, 10 ns, seemed less reasonable than the compromise value of 1 ns used in the calculations for Tables 3 and 4.

For both the A125S and V103 transducers, deconvolution of waveforms from Bph/DMH solutions with [DMH] $\leq$ 1.0 mM gave best fits with two components (no fixed parameters). The results from the A125S data gave very poorly resolved (ϕ_2^{app}, τ_2) values for these solutions (Table 3), while the V103 (ϕ_2^{app}, τ_2) values were much more clearly resolved (Table 4). This is most likely the result of the V103 transducer having a much wider bandwidth than the A125S. In addition, the V103 transducer has a lower intrinsic frequency (1.0 MHz) than does the A125S (2.25 MHz), and thus would be more responsive to

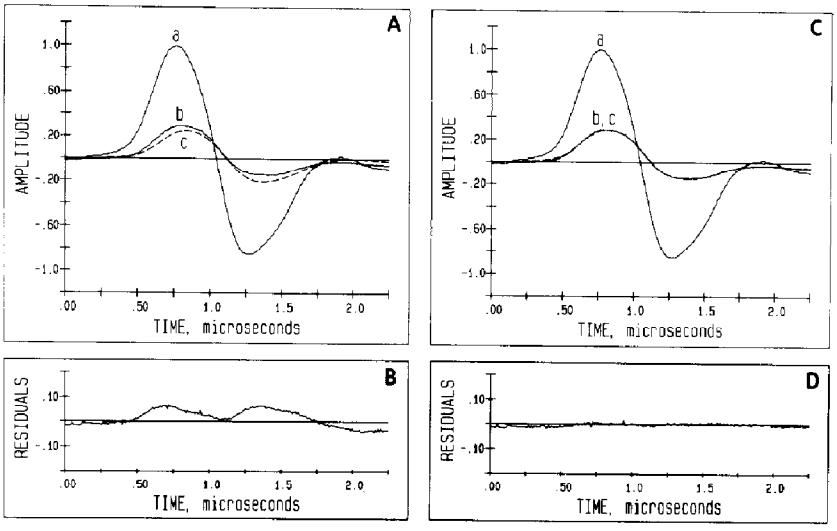

Fig. 6. One- and two-component fits of selected data from Fig. 5. In parts (A) and (C), curve (a) is ferrocene, the reference compound, and curve (b) is benzophenone in the absence of 2,5-dimethyl-2,4-hexadiene. (These are identical to curves a and b of Fig. 5B.) Part (A) shows the best one-component fit of the data, curve (c). This was generated by reconvolution with the values $\phi = 0.27$ and $\tau = 76$ ns ($\chi^2 = 1.2 \times 10^{-3}$). Part (B) shows the residuals of the data in part (A), expressed as curve (b) minus curve (c). Part (C) shows the best two-component fit of the data, curve (c). This was generated by reconvolution with the values $\phi_1 = 0.21$, $\tau_1 = 2.9$ ns, $\phi_2 = 0.47$ and $\tau_2 = 1.3$ μs ($\chi^2 = 5.8 \times 10^{-5}$). Part (D) shows the residuals of the data in part (C), expressed as curve (b) minus curve (c).

slower (μs) events [11]. That three components were not resolved is probably due to the fact that such complex resolutions are quite difficult to achieve accurately, even at much lower noise levels than were obtained here [23].

The data in Table 4, which represent the best resolution of the photochemistry occurring, can be grouped into three sets. (i) For [DMH] $\leqslant$ 0.1 mM, there is little enough diene present such that there may be significant competing quenching from the dissolved oxygen remaining after degassing by argon bubbling (expected $[O_2] \sim 10^{-6}$ to 10^{-3} M [19]). The $(\phi_1 + \phi_2)$ sum for these DMH concentrations is less than the value seen for higher DMH concentrations. Quenching of the triplet state of benzophenone by the triplet ground state of O_2 is expected to yield singlet $O_2(^1\Delta_g)$, which has a lifetime of ~ 30 μs in acetonitrile and an energy of 22.5 kcal/mol above ground state triplet [19]. The 30 μs decay is too slow to be resolvable by the V103 transducer, and the energy "tied up" by the singlet oxygen would result in $(\phi_1 + \phi_2)$ being less than unity. (ii) For [DMH] = 10 mM, only one lifetime is resolved, due to having the lifetimes for all of the reactions involved in the quenching be less than 50 ns. (iii) In the intermediate concentration region (0.1–10 mM), ϕ_1, ϕ_2 and τ_1 are roughly constant (about 0.2, 0.85 and < 10 ns, respectively), while τ_2 varies.

The interpretation of the values in Table 4 is as follows. The average of ϕ_1 for the 0–2 mM DMH data is 0.19. This ϕ value corresponds to a fast τ_1 due to the formation of the T_1 state of benzophenone. The energy of the state can be obtained from the relationship [11] $E_T = E_{h\nu}(1 - \phi_1)$, where E_T is the energy of T_1, and $E_{h\nu}$ is the photon energy (84.8 kcal/mol at 337 nm). The average value of $\phi_1 = 0.19$ gives a triplet energy of 69 kcal/mol, in excellent agreement with the literature value [24]. The second rate, τ_2, corresponds to the decay of T_1 by energy transfer to the diene and/or other processes. A Stern–Volmer plot of $1/\tau_2$ as a function of DMH concentration for 0–1 mM DMH is linear ($r^2 = 1.00$) with a slope of 7.7×10^9 M^{-1} s^{-1} and an intercept of 6.3×10^5 s^{-1} (Fig. 7). The slope corresponds to the bimolecular rate constant for

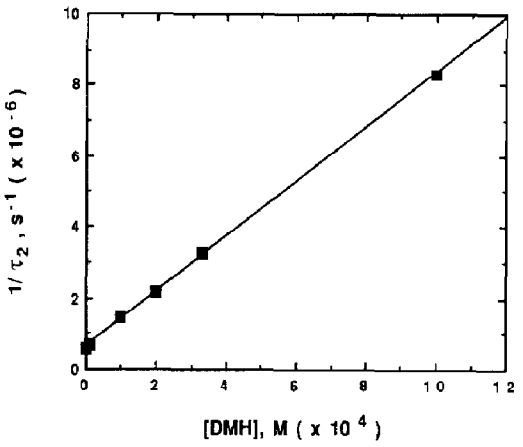

Fig. 7. Stern–Volmer plot of the quenching of triplet benzophenone by 2,5-dimethyl-2,4-hexadiene (DMH) in acetonitrile. The data are taken from Table 4.

quenching by DMH, k_q, and approaches the diffusion-controlled limit in acetonitrile. For comparison, the quenching of T_1 of benzophenone by *trans*-stilbene in acetonitrile occurs with $k_q = 7.5 \times 10^9$ M^{-1} s^{-1} [25]. The intercept indicates the lifetime of benzophenone in acetonitrile without quencher to be ~ 1.6 μs, in good agreement with the slow decay time obtained at very low quencher concentrations and in reasonable agreement with the literature value of 2.5 μs [26,27]. The latter value may be higher due to more efficient deoxygenation of the solution.

As judged by the Stern–Volmer results, τ_2 appears to adequately describe the quenching of benzophenone T_1 by DMH in the concentration region [DMH] = 0 to 2 mM. Of interest is the subsequent decay of the resulting triplet state of DMH. No third decay was resolvable from the photoacoustic data without fixing parameters. In fact, the DMH triplet is known to decay with a lifetime of ~ 44 ns [20]. Only one lifetime is resolved for very high concentrations of DMH (10 mM), Tables 3 and 4. This lifetime of 30 to 40 ns is consistent with the poor resolution of the closely spaced lifetimes of benzophenone triplet formation, benzophenone triplet quenching, and DMH triplet decay.

While not done here, it is possible [11] to incorporate sequential kinetics directly into an analysis program and be able to work with ϕ_i values directly, rather than ϕ_i^{app}. With this type of

program [11], a third decay was fixed with $\tau_3 \equiv 44$ ns and $\phi_3 \equiv 0.70$ to represent the decay of the DMH triplet. The ϕ_3 value is defined as the fraction of the photon energy released as heat for the decay of triplet DMH. Since the triplet DMH energy is 59 kcal/mol above ground state [21], this corresponds to $\phi_3 = E_T^{DMH}/E_{h\nu} = 59/84.8 = 0.70$. When the analysis was run for three components, with three fixed parameters ($\tau_1 \equiv 1$ ns, $\tau_3 \equiv 44$ ns, $\phi_3 \equiv 0.70$) for [DMH] = 0.2 to 1.0 mM, then the recovered τ_2 values [11] were within error the same as the τ_2 values in Table 3, and the recovered ϕ_2 values were about 0.10, the approximate difference between the ϕ_2 values in Table 3 and the defined $\phi_3 \equiv 0.70$ [11]. Thus, while parameters representing the decay of the quencher may be incorporated into the data analysis, little new information is obtained.

The deconvolution results of data obtained with the A125S transducer, Table 3, showed generally higher values of ϕ_1, with little resolution of a second decay. An average value of $\phi_1 = 0.22$ yields a calculated value of the benzophenone E_T of 66 kcal/mol. This is lower than the spectroscopic value of 69 kcal/mol [24]. It is not known whether the lack of resolution of a second component by this transducer may cause a distortion in the analysis results of the first component. In addition, for both transducers (Tables 3 and 4), the value of $\phi_1 + \phi_2$ is slightly greater than unity at intermediate DMH concentrations where quenching by the diene is significant. For example, for [DMH] ≥ 0.2 mM in Table 4, $\phi_1 + \phi_2$ is about 1.05. It is not known what factors, beyond the $\pm 10\%$ uncertainties in the recovered ϕ values, contribute to the value of $(\phi_1 + \phi_2)$ being greater than unity. Previously, the sum of the ϕ values for all resolved processes has been found to be closer to 1.0, thus nicely accounting for all of the absorbed photon energy [11].

6. Discussion

We have presented here the features of a computer program which quickly and successfully analyzes time-resolved photoacoustic data for sums of exponentials by means of nonlinear least squares. Of particular importance is the ability of our computer program to analyze fast lifetimes on the order of the digitization channel width, minimizing the need to fix decay parameters as done previously [11]. The fast lifetime resolution is extremely important for photacoustic data. In addition, for a given number of ϕ and τ variables, the program generally returns the same fitting parameters independent of starting guesses, provided that the starting guesses are "reasonable" (e.g., ϕ of -0.5 to 1.5, τ of 10^{-15} to 10^{-5} s for our data). Tests of the program on simulated and experimental data demonstrate that two decay components may be adequately resolved, provided that the lifetimes are within the sensitivity range of the transducer and that the experimental noise level is sufficiently low (within the range reported by most users of pulsed-laser photoacoustics).

Our strategy for developing the quadratic-fit convolution program for photoacoustics was to borrow and modify a program from the field of time-resolved fluoresence. The fluorescence nonlinear least squares program used in our laboratories is an iterative reconvolution program using the Marquardt algorithm for χ^2 minimization. It utilizes Simpson's rule approximation for the convolution integral. Specifically, the convolution integral is:

$$F_m(t) = \alpha \exp(-t/\tau) \int_0^t E_m(u) \exp(u/\tau)\, du, \tag{25}$$

where $F_m(t)$ is the measured fluorescence decay, $E_m(t)$ is the instrumental response function measured using a scatter sample, and the fluorescence impulse response is an exponential decay. The Simpson's rule for a pair of intervals in digitized data is:

$$\int_{x_0}^{x_2} f(x)\,dx \approx \frac{x_2 - x_0}{6}\left[f(x_0) + 4f(x_1) + f(x_2)\right]. \tag{26}$$

In the original Marquardt program, the integral in eq. (25) is evaluated using Simpson's rule for successive groups of data points x_0, x_1 and x_2.

The fluorescence Marquardt program was first modified to account for the fact that photoacoustic waveform analysis assumes the decay form $\phi (1/\tau) \exp(-t/\tau)$ rather than $\alpha \exp(-t/\tau)$, as used in fluorescence. This program was then used to analyze noiseless synthetic waveforms. As shown in Table 1, the program failed to accurately recover ϕ and τ values when τ was less than the digitization channel width.

The modified version of the Marquardt program we developed uses an approach different from Simpson's rule approximation. A quadratic expression is used to fit the digitized data representing the measured waveform. This results in a continuous mathematical expression for the digitized data which can be utilized in the convolution integral directly.

The qualitative differences between the two algorithms are as follows. As indicated in eq. (10), the photoacoustic convolution integral is given by $S(t) = R(t) * h(t)$, where $S(t)$ is the measured sample waveform, $R(t)$ is the measured reference waveform, and $h(t)$ is a time-dependent function representing heat release, for example. In the original convolution method, $h(t)$ is a continuous exponential function, $R(t)$ is a set of discrete points, and the convoluted function $C(t) = R(t) * h(t)$ is approximated by integration using Simpson's rule. In the quadratic-fit convolution algorithm, $h(t)$ is again a continuous exponential function, $R(t)$ is approximated as a series of continuous functions (quadratic fits to sets of discrete points, done 3 points at a time); this permits $R(t) * h(t)$ to be computed by direct integration. As shown in Table 1, the modified program performed much better than the original.

Why did the original Marquardt program fail? The difficulty in using the original Marquardt program lies in applying Simpson's rule to the convolution equation, eq. (10), for digitized photoacoustic data. The photoacoustic waveforms are obtained with a digital oscilloscope at a preset time-width per channel (or "point"; the X-axis parameter). Typically, for a 1-MHz transducer, the waveforms are digitized at 10 or 50 ns per channel, measured for 200 to 1024 channels per waveform. While the S and R functions for a 1-MHz transducer are relatively broad and can always be adequately sampled, the $h(t)$ function may be very narrow, and may not be adequately represented with 10 to 50 ns between points (the typical channel width). For example, an exponential decay with $\tau = 1$ ns results in a decay which is essentially complete in a time interval much smaller than the channel width. The method of photoacoustic waveform analysis must be able to handle $h(t)$ functions with τ values ranging from fs to s (in principle). The goal of the analysis program should be to identify fast decays as being less than the digitization channel width, without necessarily resolving the actual lifetime, and to accurately recover the preexponential ϕ factor associated with those fast decays. Algorithms for integration which might be useful for the convolution integral, such as trapezoidal integration or Simpson's rule integration, cannot be used for situations involving fast transients, as these algorithms require sufficiently close sampling points in order to accurately approximate a function.

The quadratic-fit convolution program described here is a significant improvement over the original data analysis program written by Rudzki Small and co-workers [11]. That program was important in that it showed that deconvolution of photoacoustic waveforms was possible and can yield simultaneous information on the rate and magnitude of heat release from photoinitiated reactions. However, in that early program, the methods of deconvolution utilized were relatively primitive; extensive user input was required to determine the direction of the analyses; and the analyses were very slow. The problem of analyzing fast components was dealt with accurately, but by using different algorithms for different lifetime ranges. All of these points have been improved upon by the quadratic-fit convolution program presented here.

The difficulties of the original data analysis program [11] were recognized and discussed by Melton and co-workers [13], who devised their own improved photoacoustic analysis program, utilizing the Marquardt algorithm. This program is similar to ours in that the discrete points of the reference waveform (the "T-wave") are not used directly; rather, the Melton group uses a linear

function to give the wave a functional form between data points. In our case, the reference waveform is fit with a quadratic function rather than a linear function. While the computer program written by the Melton group [13] is also a significant improvement over the original data analysis program [11], there are no data presented on the functioning of the program for decay times less than the digitization channel width.

Because the quadratic-fit convolution program was derived from a program used for fluorescence analysis, the applications of this new computer program to fluorescence data may be considered. The very fast lifetimes of importance to photoacoustics may be considered analogous to scattered light in fluorescence data. Often in nonlinear least squares fluorescence analysis, a short lifetime is fixed in an effort to account for the scatter invariably present in fluorescence data. The results we have presented suggest that there may be inaccuracies involved in using a standard nonlinear least squares program (e.g., that described by Grinvald [28] and Grinvald and Steinberg [29]) for such short lifetimes (Table 1). Indeed, Periasamy [30] has recently shown this to be true, and has developed a modified least squares program which uses a linear approximation of the successive data of the instrument response function for the computation of the convolution integral. This is similar to our method, although we have used a quadratic approximation rather than a linear approximation.

While the photoacoustic nonlinear least squares analyses presented here are similar to fluorescence analyses, there are some differences in the details of the evaluation of goodness of fit. In fluorescence analyses, it is usual to weight the residuals in χ^2 calculations [17,28,29], yielding a more statistically correct analysis and giving χ^2 values which tend toward unity for good fits. Here, we have not yet implemented weighting factors, which would require the estimation of variance for photoacoustic data, a function of the experimental noise. Thus, the χ^2 values reported here have a wide range of magnitudes, all less than 1.0. Future work is required for the estimation of the variance for instrumental noise on photoacoustic waveforms.

By beginning to utilize fluorescence data analysis methods for photoacoustic waveform analysis, we have started to exploit the sophistication which exists in the field of time-resolved fluorescence decay. The obvious next step in the implementation of nonlinear least squares is the use of global and target analysis for the discrimination of enthalpic, volumetric and kinetic information from photoacoustic waveforms. This may be done using eq. (4) and the methods of global analysis worked out by Knutson, Beechem and Brand [31,32]. Additionally, transform methods such as the Method of Moments appear very successful for photoacoustics and are actively being developed and utilized [23,33].

Conclusions

We have developed a nonlinear least squares computer program which rapidly deconvolves photoacoustic data while minimizing the need for fixing parameters. The program utilizes the Marquardt algorithm for χ^2 minimization and a quadratic-fit method for evaluating the convolution integral. The quadratic-fit method is an improvement over Simpson's rule integration approximation, which did not allow accurate recovery of ϕ parameters for lifetimes less than the digitization channel width. Studies with simulated data in the absence of noise show that the quadratic-fit convolution program accurately returns the ϕ preexponential factor, even when the associated lifetime is less than the digitization channel width. With synthetic noise added to simulated waveforms in the amount of 0.01 standard deviation (slightly higher than the level usually seen experimentally), two component resolutions (four independent parameters) are easily achieved.

The computer program was tested using experimental data from the quenching of benzophenone triplet by a diene quencher in acetonitrile. One or two decay components were resolved depending on the concentration of the diene and

the transducer used for detection. The heavily damped, broadband, 1 MHz transducer was more sensitive to the experimental decay components than the narrowband 2.25 MHz transducer. Analysis of the data from the benzophenone/diene system gave good results for the benzophenone triplet energy, lifetime, and quenching constant, and were consistent with a short lifetime for the excited state of the diene quencher.

Acknowledgments

JRS would like to thank Dr. Ludwig Brand for many helpful discussions on approaches to photoacoustic waveform deconvolution, and Dr. John E. Rudzki, Jr. for first pointing out the appearance of convolution effects in photoacoustic data. We thank Drs. Jay R. Knutson and Joseph M. Beechem for many helpful discussions. Janet Lee performed some of the initial programming work. Shane L. Larson provided expert computer programming and technical assistance. Jonathan J. Hutchings and Irana W. Hawkins performed some of the analyses of simulated waveforms. The original Marquardt computer program used in our laboratories was obtained from Dr. Bruce Hudson's laboratory at the University of Oregon. We thank Panametrics, Inc., for generously supplying transducers for demonstration purposes. The work of JRS was possible through support from the National Institutes of Health (GM-41415 and GM-10889), the National Science Foundation (DMB-8707705), the Medical Research Foundation of Oregon, and Tektronix, Inc. EWS received support from the National Institutes of Health (GM-25663).

References

1 S.E. Braslavsky and K. Heihoff, in: CRC Handbook of organic photochemistry, ed. J.C. Scaiano, vol. I (CRC Press, Boca Raton, FL, 1989) p. 327.
2 A.C. Tam, Rev. Mod. Phys. 58 (1986) 381.
3 K.S. Peters and G.J. Snyder, Science. 241 (1988) 1053.
4 S.E. Braslavsky, Ber. Bunsenges. Phys. Chem. 93 (1989) 356.
5 S.E. Braslavsky, in: Photoacoustic and photothermal phenomena, eds. P. Hess and J. Pelzl, vol. 58 (Springer-Verlag, Berlin, 1988) p. 508.
6 K.S. Peters, T. Watson and K. Marr, in: Annual reviews of biophysics and biophysical chemistry, eds. D.M. Engelman, C.R. Cantor and T.D. Pollard, vol. 20 (Annual Reviews, Inc., Palo Alto, CA, 1991) p. 343.
7 M.S. Herman and J.L. Goodman, J. Am. Chem. Soc. 111 (1989) 1849.
8 W.P. Leung, K.C. Cho, S.K. Chau and C.L. Choy, Chem. Phys. Letts. 141 (1987) 220.
9 J.A. Westrick and K.S. Peters, Biophys. Chem. 37 (1990) 73.
10 J.A. Westrick, K.S. Peters, J.D. Ropp and S.G. Sligar, Biochemistry 29 (1990) 6741.
11 J.E. Rudzki, J.L. Goodman and K.S. Peters, J. Am. Chem. Soc. 107 (1985) 7849.
12 K. Heihoff and S.E. Braslavsky, Chem. Phys. Lett. 131 (1986) 183.
13 L.A. Melton, T. Ni and Q. Lu, Rev. Sci. Inst. 60 (1989) 3217.
14 P.R. Bevington, Data reduction and error analysis for the physical sciences (McGraw-Hill, New York, NY, 1969) p. 336.
15 J.E. Rudzki, L.J. Libertini and E.W. Small, Biophys. J. 53 (1988) 395a.
16 J.R. Small and S.L. Larson, in: Time-resolved laser spectroscopy in biochemistry II, ed. J.R. Lakowicz, vol. 1204 (Society of Photo-Optical Instrumentation Engineers, Bellingham, WA, 1990) p. 126.
17 D.A. Holden, in: CRC Handbook of organic photochemistry, ed. J.C. Scaiano, vol. I (CRC Press, Boca Raton, FL, 1989) p. 261.
18 L.J. Rothberg, J.D. Simon, M. Bernstein and K.S. Peters, J. Am. Chem. Soc. 105 (1983) 3464.
19 N.J. Turro, Modern molecular photochemistry (Benjamin/Cummings, Menlo Park, CA, 1978) p. 628.
20 R.A. Caldwell and M. Singh, J. Am. Chem. Soc. 104 (1982) 6121.
21 S.L. Murov, Handbook of photochemistry (Marcel Dekker, Inc., New York, NY, 1973) p. 272.
22 G.L. Geoffroy and M.S. Wrighton, Organometallic photochemistry (Academic Press, New York, NY, 1979) p. 335.
23 E.W. Small, L.J. Libertini, D.W. Brown and J.R. Small, in: Fluorescence detection III, ed. E.R. Menzel, vol. 1054 (Society of Photo-Optical Instrumentation Engineers, Bellingham, WA, 1989) p. 36.
24 W.G. Herkstroeter, A.A. Lamola and G.S. Hammond, J. Am. Chem. Soc. 86 (1964) 4537.
25 W.D.K. Clark and C. Steel, J. Am. Chem. Soc. 93 (1971) 6347.
26 W.D.K. Clark, A.D. Litt and C. Steel, J. Am. Chem. Soc. 91 (1969) 5413.
27 L. Giering, M. Berger and C. Steel, J. Am. Chem. Soc. 96 (1974) 953.
28 A. Grinvald, Anal. Biochem. 75 (1976) 260.

29 A. Grinvald and I.Z. Steinberg, Anal. Biochem. 59 (1974) 583.
30 N. Periasamy, Biophys. J. 54 (1988) 961.
31 J.M. Beechem, in: Numerical computer methods, eds. L. Brand and M.L. Johnson, Methods in Enzymology Vol. 210 (Academic Press, San Diego, CA, 1991) in press.
32 J.R. Knutson, J.M. Beechem and L. Brand, Chem. Phys. Lett. 102 (1983) 501.
33 J.R. Small, S.H. Watkins, B.J. Marks and E.W. Small, in: Time-resolved laser spectroscopy in biochemistry II, ed. J.R. Lakowicz, vol. 1204 (Society of Photo-Optical Instrumentation Engineers, Bellingham, WA, 1990) p. 231.